# Dynamic spectral-domain optical coherence elastography for tissue characterization

**Xing Liang,[1,2] Steven G. Adie,[2] Renu John,[2] and Stephen A. Boppart[1,2,3,*]**

[1]*Department of Electrical and Computer Engineering, 405 N. Mathews Avenue, Urbana, IL 61801, USA*
[2]*Beckman Institute of Advanced Science and Technology, 405 N. Mathews Avenue, Urbana, IL 61801, USA*
[3]*Departments of Bioengineering, and Medicine, University of Illinois at Urbana-Champaign, 405 N. Mathews Avenue, Urbana, IL 61801, USA*
**boppart@illinois.edu*

**Abstract:** A dynamic spectral-domain optical coherence elastography (OCE) imaging technique is reported. In this technique, audio-frequency compressive vibrations are generated by a piezoelectric stack as external excitation, and strain rates in the sample are calculated and mapped quantitatively using phase-sensitive spectral-domain optical coherence tomography. At different driving frequencies, this technique provides contrast between sample regions with different mechanical properties, and thus is used to mechanically characterize tissue. We present images of a three-layer silicone tissue phantom and rat tumor tissue *ex vivo*, based on quantitative strain rate. Both acquisition speed and processing speed are improved dramatically compared with previous OCE imaging techniques. With high resolution, high acquisition speed, and the ability to characterize the mechanical properties of tissue, this OCE technique has potential use in non-destructive volumetric imaging and clinical applications.



**OCIS codes:** (110.4500) Optical coherence tomography; (120.5820) Scattering measurements; (120.5050) Phase measurement; (170.6935) Tissue characterization.

## References and links

1. J. M. Schmitt, "OCT elastography: imaging microscopic deformation and strain of tissue," Opt. Express **3**(6), 199–211 (1998).
2. M. Orescanin, K. S. Toohey, and M. F. Insana, "Material properties from acoustic radiation force step response," J. Acoust. Soc. Am. **125**(5), 2928–2936 (2009).
3. H. J. Ko, W. Tan, R. Stack, and S. A. Boppart, "Optical coherence elastography of engineered and developing tissue," Tissue Eng. **12**(1), 63–73 (2006).
4. R. K. Wang, Z. H. Ma, and S. J. Kirkpatrick, "Tissue Doppler optical coherence elastography for real time strain rate and strain mapping of soft tissue," Appl. Phys. Lett. **89**(14), 144103 (2006).
5. X. Liang, A. L. Oldenburg, V. Crecea, E. J. Chaney, and S. A. Boppart, "Optical micro-scale mapping of dynamic biomechanical tissue properties," Opt. Express **16**(15), 11052–11065 (2008).
6. S. G. Adie, B. F. Kennedy, J. J. Armstrong, S. A. Alexandrov, and D. D. Sampson, "Audio frequency *in vivo* optical coherence elastography," Phys. Med. Biol. **54**(10), 3129–3139 (2009).
7. B. F. Kennedy, T. R. Hillman, R. A. McLaughlin, B. C. Quirk, and D. D. Sampson, "*In vivo* dynamic optical coherence elastography using a ring actuator," Opt. Express **17**(24), 21762–21772 (2009).
8. X. Liang, M. Orescanin, K. S. Toohey, M. F. Insana, and S. A. Boppart, "Acoustomotive optical coherence elastography for measuring material mechanical properties," Opt. Lett. **34**(19), 2894–2896 (2009).
9. X. Liang, and S. A. Boppart, "Biomechanical properties of *in vivo* human skin from dynamic optical coherence elastography," IEEE Trans. Biomed. Eng. (to be published).
10. V. Crecea, A. L. Oldenburg, X. Liang, T. S. Ralston, and S. A. Boppart, "Magnetomotive nanoparticle transducers for optical rheology of viscoelastic materials," Opt. Express **17**(25), 23114–23122 (2009).
11. M. A. Kasapi, and J. M. Gosline, "Strain-rate-dependent mechanical properties of the equine hoof wall," J. Exp. Biol. **199**(Pt 5), 1133–1146 (1996).
12. F. Jamal, J. Strotmann, F. Weidemann, T. Kukulski, J. D'hooge, B. Bijnens, F. Van de Werf, I. De Scheerder, and G. R. Sutherland, "Noninvasive quantification of the contractile reserve of stunned myocardium by ultrasonic strain rate and strain," Circulation **104**(9), 1059–1065 (2001).
13. X. Liang, and S. A. Boppart, "Dynamic optical coherence elastography and applications, " in *Asia Communications and Photonics Conference and Exhibition*, Technical Digest (CD) (Optical Society of America, 2009), paper TuG2.

#126681 - $15.00 USD Received 7 Apr 2010; revised 8 Jun 2010; accepted 14 Jun 2010; published 16 Jun 2010

14. B. W. Pogue, and M. S. Patterson, "Review of tissue simulating phantoms for optical spectroscopy, imaging and dosimetry," J. Biomed. Opt. **11**(4), 041102 (2006).
15. R. John, R. Rezaeipoor, S. G. Adie, E. J. Chaney, A. L. Oldenburg, M. Marjanovic, J. P. Haldar, B. P. Sutton, and S. A. Boppart, "*In vivo* magnetomotive optical molecular imaging using targeted magnetic nanoprobes," Proc. Natl. Acad. Sci. U.S.A. **107**(18), 8085–8090 (2010).
16. R. A. Leitgeb, and M. Wojtkowski, "Complex and coherence noise free Fourier domain optical coherence tomography, " in *Optical Coherence Tomography: Technology and Applications,* W. Drexler and J.G. Fujimoto, Eds. (Springer, New York, 2008).

## 1. Introduction

Optical coherence elastography (OCE) is an imaging technique that can determine sample mechanical properties utilizing optical coherence tomography (OCT) [1]. At both the microscopic scale and mesoscopic scale, OCE plays a significant role for measuring and imaging tissue mechanical properties in biological and clinical applications, because of its inherent features of micron-scale resolution, millimeter-scale penetration depth, and non-destructive imaging capability. Like its counterpart ultrasound elastography [2], recent efforts in OCE research have utilized dynamic excitation methods. In contrast to quasi-static OCE techniques [3], dynamic OCE techniques have used mechanical waves for excitation, being applied to the sample either internally or externally to avoid complex boundary conditions and the inaccuracies associated with speckle tracking methods. Doppler OCE was first introduced to map velocity, displacement, and strain rate in a phantom using a spectral-domain OCT system and quasi-static mechanical compression [4]. Quantitative tissue characterization was later achieved by a dynamic OCE method which mapped human tumor tissue for relative elastic moduli [5]. Dynamic OCE was also performed using time-domain OCT systems based on a Bessel frequency spectrum of the interferometric OCT signal [6,7]. However, the applicability of these dynamic OCE techniques for real-time or *in vivo* diagnostics is limited by their data acquisition and processing speeds. Time-domain dynamic OCE inherently operates at slow image acquisition rates, while previous spectral-domain dynamic OCE mapping technique needs a long acquisition time by taking M-mode OCT images per transverse location and a long curve-fitting processing time [5–7]. In dynamic OCE, mechanical compression is usually applied as the excitation method, but other excitation methods such as surface wave propagation and internal acoustomotive or magnetomotive excitations have also been applied in OCE to characterize mechanical properties of samples [8–10].

In this paper, we report a novel dynamic OCE technique to image biomechanical properties of tissue that combines dynamic mechanical excitation with fast image acquisition and processing. B-mode images were acquired during sinusoidal mechanical compression excitation, and local strain rates were calculated to represent local biomechanical properties. Different excitation frequencies were used to highlight sample regions with distinct mechanical properties. Results were obtained from tissue phantoms and rat tumor tissues *ex vivo*. This technique features fast image acquisition and processing speeds, and therefore has the potential for non-destructive volumetric imaging and clinical applications.

## 2. Materials and methods

### *2.1 Experimental setup*

The OCE system, as shown in Fig. 1, was constructed based on a spectral-domain OCT system which used a Nd:$YVO_4$-pumped titanium:sapphire laser as broad-band source, providing a center wavelength of 800 nm and a bandwidth of 100 nm. The full-width half-maximum axial and transverse resolutions of the OCT system were approximately 3 μm and 13 μm respectively. The average power incident on the samples was 10 mW. For the OCE sample arm, a fixed 2° round wedge prism (PS810-B, Thorlabs, Newton, NJ) was used to restrict the upper boundary of the sample, and a piezoelectric (PZT) stack (AE0505D16F, Thorlabs, Newton, NJ) was used to bound the bottom of the sample. The PZT stack was driven by a single channel PZT driver (MDT694, Thorlabs, Newton, NJ) and used to sinusoidally displace the sample under frequencies of 20 Hz, 45 Hz, 100 Hz, and 313 Hz in

#126681 - $15.00 USD Received 7 Apr 2010; revised 8 Jun 2010; accepted 14 Jun 2010; published 16 Jun 2010

the axial direction. Minimal contact and force were applied to the samples prior to data acquisition and a 30 $V_{pp}$ sinusoidal voltage signal was applied to the PZT stack during data acquisition, providing 4.5 µm maximum displacement. The axial depth scans in the OCE images were collected by a CCD line-scan camera at acquisition line rates of 1 kHz and 10 kHz. The camera acquisition was synchronized with a transverse scanning galvanometer and the PZT stack excitation.

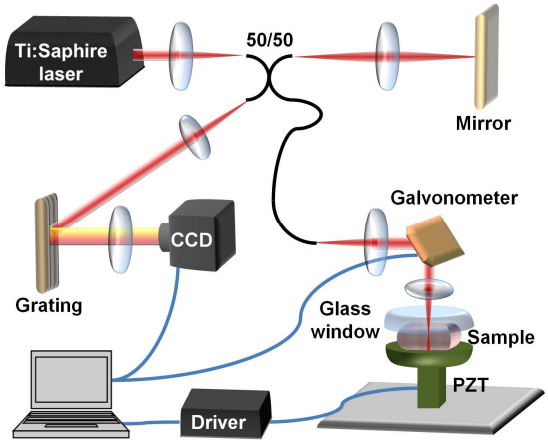


Fig. 1. Schematic diagram of the dynamic spectral-domain OCE system. In the sample arm of the OCE system, the glass window is rigidly fixed to the table. The PZT (piezoelectric stack) is synchronized with data acquisition, and compresses the sample against the glass window.

*2.2 Data acquisition and processing*

OCE images were computed from B-mode OCT spectral data sets acquired during dynamic mechanical excitation and acquired with no mechanical excitation. In the transverse direction of the images, a number of cycles of sinusoidal oscillations from the samples were recorded according to the excitation frequency. These oscillations inside the samples were caused by the external excitation, and their amplitudes were determined by both the excitation amplitude and the local mechanical properties of the samples. To extract the mechanical properties of the samples, a custom processing algorithm (Fig. 2) was used to analyze the OCE images. First, the reference background OCT image was subtracted from the data sets, and fast Fourier transformations were taken for each column of the data sets to calculate the complex OCT signals from the spectral data. The phase was then calculated for each corresponding pixel of the signal, and the phase difference between adjacent A-lines was computed, which was proportional to the scatterer velocities in the axial direction. The phase unwrapping along the transverse dimension was then performed and fast Fourier transformations were taken in the transverse direction to obtain the lateral phase evolution as the motion spectrum. A bandpass filter at the driving frequency and with an appropriate bandwidth was used to select the sample motion under each driving frequency. Thus, after inverse fast Fourier transformation, the sample motion velocities under the driving frequencies were extracted in the OCE phase signal for each pixel. Finally, strain rate calculations and down sampling were applied to generate the OCE images. To improve specificity, the strain rate images were divided by the ones without any mechanical excitation, and shown in decibels. From the OCE data processing, amplitudes of vibration strain rates of the samples under driving frequencies in the sample were extracted for the OCE images. The strain rates can be expressed as

$$\varepsilon'(x,z) = \frac{\Delta\phi(x,z)\bar{\lambda}}{4\pi n\tau(z-z_0)}, \tag{1}$$

#126681 - $15.00 USD Received 7 Apr 2010; revised 8 Jun 2010; accepted 14 Jun 2010; published 16 Jun 2010

where $x$ and $z$ denote the lateral and the axial direction, respectively, $\Delta\phi$ is the phase difference between each adjacent A-lines, $\bar{\lambda}$ is the central wavelength of the source, $\tau$ is the time interval between two adjacent A-lines, and $z_0$ is the surface of the sample.

Strain rate is an important parameter for characterizing the local mechanical properties of samples. It is related to measurements of moduli [11] and has been widely used for ultrasound myocardial imaging [12]. Strain rate is the rate by which the deformation occurs, and can be described by $\varepsilon' = \delta\varepsilon / \delta t$, where □ is the strain. The strain rate at depth $z$ is effectively an average of the strain rates along the axial line beginning at $z_0$. We use the division factor $(z\text{-}z_0)$ to detect the local discontinuity of mechanical property variation. Under dynamic excitations, the strain rate variations are frequency dependent, and may represent local discontinuities or contrasts within one A-line, because local strain rate at resonance frequency increase amplitude dramatically. The excitation frequencies in this OCE technique were chosen to be around the previous determined resonant frequencies for the investigated samples, which were obtained using the dynamic OCE method described in a previous study [13], for both the tissue phantom and the rat tissue. However, these chosen frequencies may be different from the calibrated resonant frequency for a particular tissue type because of the complexity of the sample geometry, boundary conditions and potential mechanical coupling between the sample and experimental mounting hardware. For example, the resonant frequency of rat adipose tissue was found to be ~39 Hz from the previous study [13], but in this study, we found a 45 Hz excitation frequency to be the most effective frequency to generate the greatest contrast for the adipose tissue.

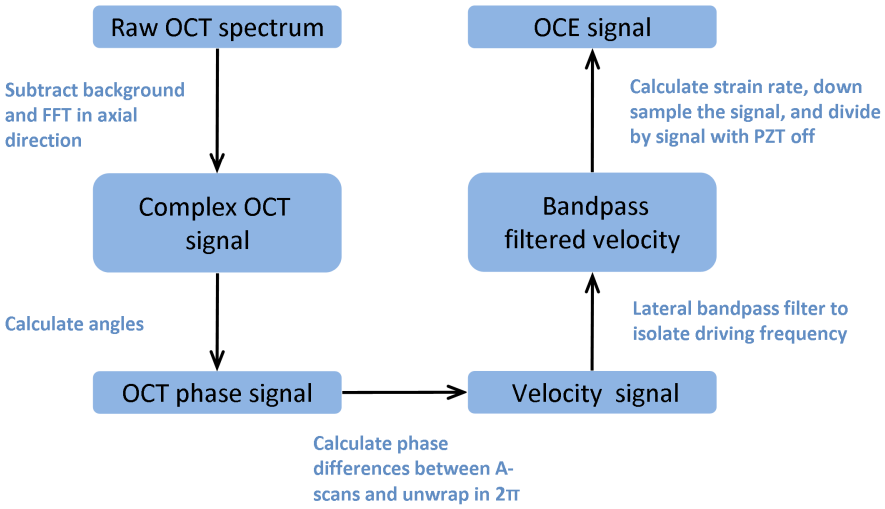


Fig. 2. OCE signal processing flow chart.

### *2.3 Data acquisition constraints and system resolution*

The excitation frequencies are also limited by the axial scan rate, since the axial scan rate must be sufficiently fast to sample the excitations. This can be described as $f_A > 2f_E$, where $f_A$ is axial scan rate and $f_E$ is the excitation frequency. In this study, we have utilized 4 excitation frequencies (20 Hz, 45 Hz, 100 Hz, and 313 Hz). For the first three excitation frequencies, $f_A$ = 1 kHz was used. However, for the 313 Hz excitation frequency, an $f_A$ of 1 kHz was too close to $2f_E$ by the Nyquist criterion, and thus an $f_A$ of 10 kHz was used. The CCD exposure time was set to be 100 μs for both axial scan rates, so that the imaging sensitivities were the same for all experiments, regardless of the excitation frequency.

#126681 - $15.00 USD Received 7 Apr 2010; revised 8 Jun 2010; accepted 14 Jun 2010; published 16 Jun 2010

The axial resolution of this OCE technique is the same as for OCT, which is the optical source coherence length. However, the transverse resolution of this OCE technique may be different, and is the larger value between the transverse OCT resolution and the resolution given by:

$$R_{OCE} = m \cdot d = \frac{f_A}{f_E} \cdot \frac{\Delta x}{N}, \tag{2}$$

where $\Delta x$ is the transverse scanning range, $N$ is the number of axial scans in the raw OCT spectral data, $d$ is the effective scanning distance for each A-line, and $m = f_A / f_E$ is the down sampling factor. The calculated OCE lateral resolution corresponds to the effective scanning distance for each mechanical vibration cycle. One example is for the rat tumor tissue experiment. When $f_A$ is 1 kHz, $f_E$ is 45 Hz, $\Delta x$ is 2 mm, $N$ is 4000, the down sampling factor is 22, the effective scanning distance for each A-line is 0.5 μm, and the interval for each A-scan is 1 ms, as shown in Fig. 3(a). Therefore $R_{OCE}$ is 11 μm as calculated from Eq. (2). However, limited by the beam spot size, the transverse OCE resolution cannot be smaller than the transverse OCT resolution. Therefore, the effective OCE transverse resolution is 13 μm for this example. If $f_A$ is doubled to 2 kHz, $f_E$ is 45 Hz, $\Delta x$ is 2 mm, and $N$ is 4000, the interval for each A-scan is 0.5 ms, and thus the down sampling factor is 44. The effective scanning distance for each A-line remains unchanged to be 0.5 μm. Therefore, $R_{OCE}$ is 22 μm as calculated from Eq. (2), which is larger than and thus not limited by the OCT transverse resolution. For this example, the effective transverse OCE resolution is 22 μm, as shown in Fig. 3(b). If $f_A$ is 1 kHz, $f_E$ is 45 Hz, $\Delta x$ is 2 mm, but $N$ is 2000, the down sampling factor is 22, the effective scanning distance for each A-line is 1 μm, and the interval for each A-scan is 1 ms. The effective transverse OCE resolution is also 22 μm, as calculated by Eq. (2) and shown in Fig. 3(c).

*2.4 Sample preparation*

Samples imaged by OCE in this study included 3-layer silicone tissue phantoms and rat tumor tissues. Silicone-based tissue phantoms were fabricated from pure polydimethylsiloxane (PDMS) fluid (50 cSt viscosity, ClearCo, Inc.), a room-temperature vulcanizing silicone, and the associated curing agent (General Electric RTV-615 A and B, respectively, Circuit Specialists, Inc.). Two concentration ratios of these three ingredients were used to obtain two different elastic moduli in the layers of the samples, which were 1:10:20 and 1:10:80 corresponding to elastic moduli of approximately 100 kPa and 10 kPa based on previous calibration studies [5]. Polystyrene microspheres (mean diameter 0.53 μm, Bangs Laboratories, Inc.) were embedded in the tissue phantoms with a concentration of 1 mg/g to function as optical scatterers for OCE imaging. Phantoms with polystyrene microspheres have relatively deeper penetration depth for OCT imaging due to smaller refractive index variations [14]. The phantom solutions were mixed thoroughly in an ultrasonicator for 30 minutes under room temperature and then poured into 9 cm plastic Petri dishes. Different layers of samples with different elastic moduli and thicknesses were fabricated separately after the curing process of the previous layer, which includes curing at 80°C for 8 hours and subsequently at room temperature for 24 hours. The silicone tissue phantoms were sectioned into cubes of dimensions approximately 8 mm × 8 mm × 3 mm (x-y-z directions) for OCE imaging.

Female inbred Wistar–Furth rats (6-8 weeks old) (Harlan, Indianapolis, IN) were also used in this study. Experiments were performed under a protocol approved by the Institutional Animal Care and Use Committee at the University of Illinois at Urbana-Champaign. The rats were individually housed, fed standard rat chow pellets, provided with water and food ad libitum, and kept on a 12-hr light–dark cycle. The induction of mammary tumors using the carcinogen N-methyl-N-nitrosourea (MNU) (50 mg/kg) was done as previously described [15]. Briefly, the MNU was injected intraperitoneally in the left side of the peritonea. A second injection of MNU into the right side of the peritonea was administered 7 days later. Following MNU injections, animals were palpated weekly to determine mammary tumor

#126681 - $15.00 USD Received 7 Apr 2010; revised 8 Jun 2010; accepted 14 Jun 2010; published 16 Jun 2010

development. Tumor with surrounding adipose tissues was excised and resected into cubic shapes with approximate dimensions of 4 mm × 3 mm × 3 mm for OCE imaging.

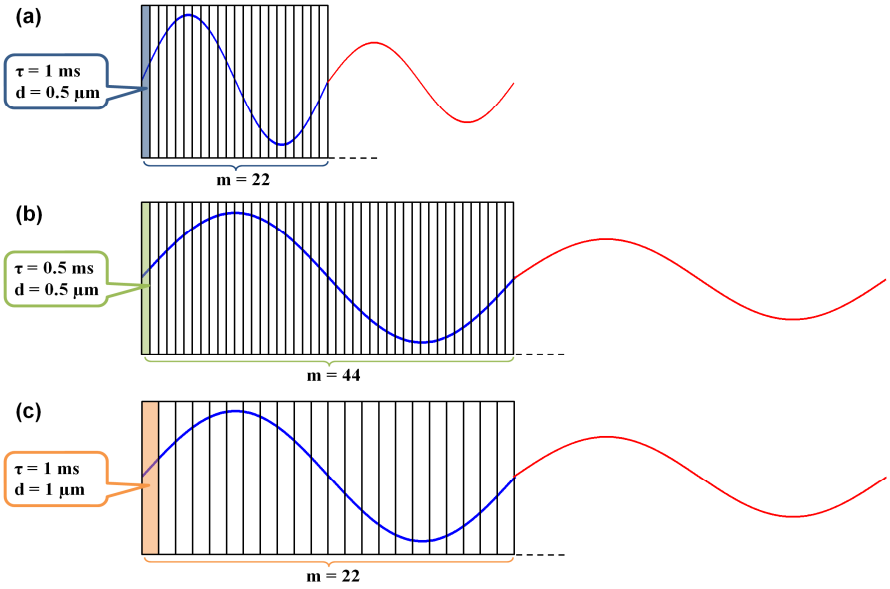


Fig. 3. Dependence of OCE lateral resolution on data acquisition parameters. The horizontal axis of the illustrations display the sampling of the acquired OCT image in lateral spatial coordinates. (a) OCE lateral resolution when $f_A$ is 1 kHz, $f_E$ is 45 Hz, $\Delta x$ is 2 mm, and $N$ is 4000. (b) OCE lateral resolution when $f_A$ is 2 kHz, $f_E$ is 45 Hz, $\Delta x$ is 2 mm, and $N$ is 4000. (c) OCE lateral resolution when $f_A$ is 1 kHz, $f_E$ is 45 Hz, $\Delta x$ is 2 mm, and $N$ is 2000.

## 3. Results and discussion

This dynamic spectral-domain OCE technique was first applied on the 3-layer tissue phantoms. In the tissue phantom illustrated here, the top layer had an elastic modulus of ~100 kPa and a thickness of ~200 µm. The middle layer had an elastic modulus of ~10 kPa and a thickness of ~400 µm, and the bottom layer had an elastic modulus of ~100 kPa and a thickness of ~2400 µm, which is shown in the structural OCT image in Fig. 4(a). The OCE images under driving frequencies of 20 Hz and 100 Hz are shown in Fig. 4(b) and 4(c) (green channel), with the structural OCT image as the background (red channel). Under 20 Hz excitation, the OCE signal is shown predominantly in the middle layer. When the excitation frequency is increased to 100 Hz, the OCE signal is shown predominantly in the top and middle layers.

Strain rates as calculated in Eq. (1) and shown in the OCE images are used to differentiate mechanical properties under different driving frequencies. If the mechanical properties of samples result in resonance at a given driving frequency, the vibration strain rates will increase. This feature of OCE imaging may be used to mechanically characterize specific regions within heterogeneous samples. For OCE using 20 Hz excitation, the strain rate of the soft middle layer is relatively high, suggesting it is near resonance. The stiff top layer is not effectively compressed, suggesting it is far from resonance. The OCE image therefore has a low strain rate in this top layer. The low strain rate in the bottom layer suggests that it is also off resonance, but is nevertheless transmitting vibrations to the middle layer. Thus in the OCE image, appreciable strain rate values are observed. However, the OCT signal for the bottom layer also has lower SNR compared to the other two layers, and the resulting higher phase noise causes attenuation of the OCE signal in this layer, at both excitation frequencies [16].

#126681 - $15.00 USD Received 7 Apr 2010; revised 8 Jun 2010; accepted 14 Jun 2010; published 16 Jun 2010

For OCE at 100 Hz excitation, larger strain rate values with bulk motion in the top and bottom layers suggest that the top and bottom layers are close to a resonance.

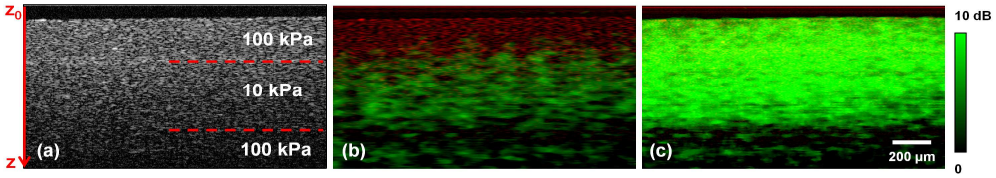


Fig. 4. OCT and OCE images of a three-layer tissue phantom. (a) Structural OCT image. Young's moduli are labeled for each corresponding layer. The red axis denotes the A-scan direction and the dotted lines denote the boundaries of the layers. (b) OCE image under 20 Hz mechanical excitation. (c) OCE image under 100 Hz mechanical excitation. Scale bar applies to all the images.

The OCE results from rat tumor tissue are shown in Fig. 5. Figure 5(a) and 5(c) are the OCE images of the tissue under 45 Hz and 313 Hz excitations, respectively. The corresponding OCT structural image and histological image are shown in Fig. 5(b) and 5(d), respectively. From Fig. 5, one can observe that under 45 Hz excitation, the OCE image highlights predominantly the adipose tissue region (left side of image), while under 313 Hz, the OCE image highlights predominantly the tumor tissue region (right side of image). The 45 Hz and 313 Hz frequencies are near the previously measured mechanical resonances for rat adipose and tumor tissue [13], respectively. Therefore in the heterogeneous rat tumor tissue, different tissue types were selectively highlighted under different driving frequencies according to their different resonances. Furthermore, in Fig. 5(a), the OCE image includes two regions from the right side (orange arrows) which corresponds to the highly scattering region from the OCT signal in Fig. 5(b). From the histological image in Fig. 5(d), it is shown that this region corresponds to local areas of adipose cells and connective tissues (orange arrows) within the tumor, which is poorly differentiated from the OCT scattering image. On the other hand, in Fig. 5(c), the OCE image includes some regions from the left side (blue arrow) which corresponds to the low scattering region from the OCT signal in Fig. 5(b). According to the histological image in Fig. 5(d), those regions correspond to invading tumor tissues in the adipose side (blue arrow).

The image acquisition and processing speeds of this OCE technique have been dramatically improved compared with the previous studies [5–7]. The acquisition speed is 4 s per frame for a 1 kHz axial scan rate and 0.8 s per frame for a 10 kHz axial scan rate. The processing speed is approximately 1 s per frame using Matlab on a PC with a dual core 2.0 GHz AMD Athlon™ CPU and 2 Gigabytes of memory. With these higher acquisition and processing rates, this dynamic OCE technique has the potential for volumetric biomechanical imaging, and with state-of-the-art OCT hand held probes, there is also the potential for non-destructive *in vivo* and clinical applications using a ring actuator design [7].

#126681 - $15.00 USD Received 7 Apr 2010; revised 8 Jun 2010; accepted 14 Jun 2010; published 16 Jun 2010

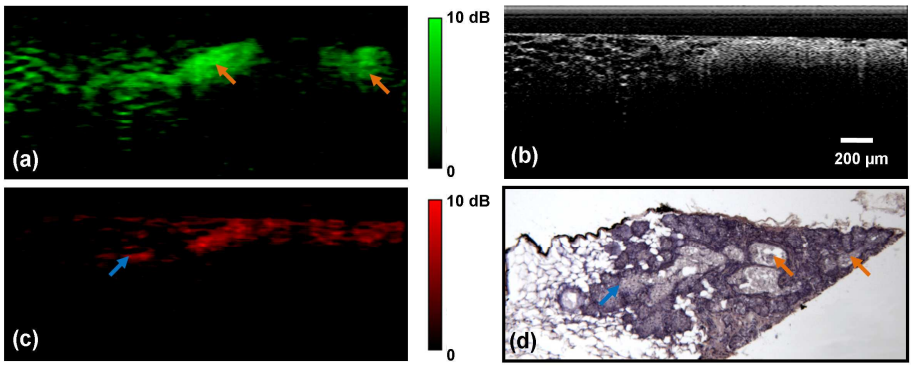


Fig. 5. OCE results on *ex vivo* rat tumor tissue. (a) OCE image under 45 Hz mechanical excitation. (b) OCT structural image of the tissue. (c) OCE image under 313 Hz mechanical excitation. (d) Corresponding histological image. Scale bar applies to all the images. Arrows are discussed in the text.

## 4. Conclusion

A dynamic OCE technique has been demonstrated based on a phase-sensitive spectral-domain OCT system and audio-frequency external mechanical excitations. It provides micron-scale resolution, fast imaging and processing speeds, and non-destructive biomechanical imaging capability. Based on local mechanical properties, this technique has shown the ability to differentiate sample regions in silicone tissue phantoms and rat tumor tissues under different excitation frequencies, using strain rate as contrast. Ongoing studies are aimed at conducting *in vivo* measurements and investigating the potential for characterizing the full frequency-dependant mechanical response of tissues.

## Acknowledgments

We thank Professor Amy L. Oldenburg for her insightful discussions regarding algorithm development. We also thank Dr. Haohua Tu and Eric J. Chaney for their laboratory assistance. This work was supported in part by the National Institutes of Health (NIBIB, R01 EB005221, R01 EB009073, and NCI RC1 CA147096, S.A.B.). Additional information can be found at http://biophotonics.illinois.edu.

#126681 - $15.00 USD Received 7 Apr 2010; revised 8 Jun 2010; accepted 14 Jun 2010; published 16 Jun 2010